Effective removal of water-soluble methylated arsenic contaminants with phosphorene oxide nanoflakes: A DFT study

Kerry Wrighton-Araneda[1], *Daniela E. Ortega*[2], *Diego Cortés-Arriagada*[1,*]

[1]Programa Institucional de Fomento a la Investigación, Desarrollo e Innovación, Universidad Tecnológica Metropolitana, Ignacio Valdivieso, 2409, 8940577, San Joaquín, Santiago, Chile. *E-mail address: dcortes@utem.cl

[2]Centro Integrativo de Biología y Química Aplicada (CIBQA), Universidad Bernardo O'Higgins, General Gana 1702, Santiago, 8370854, Chile

Abstract. This work explores by density functional theory calculations the ability of oxidized phosphorene nanoflakes (PhosO) to simultaneously remove methylarsenicals from contaminated water sources via adsorption in solid phases. Adsorption energies and conformations, energy decomposition analyses (ALMO-EDA), binding analyses, implicitly/explicitly solvated structures, and competitive adsorption with coexisting molecules afford deep insights into the selectivity adsorption and interaction mechanisms. The PhosO nanoflakes form inner-sphere surface complexes with methylarsenicals underwater conditions, even with enhanced adsorption stability compared to intrinsic phosphorene and without the competition of water molecules for adsorption sites. The inner-sphere surface adsorption of trivalent methylarsenicals is driven by electrostatic forces and contributed from charge-transfer (orbital) stabilization. While surface complexation of pentavalent methylarsenicals occurs by a balanced contribution of orbital and long-range driving forces, explaining their relative higher adsorption energies than trivalent pollutants; anionic contaminants also show a high stabilization via extra polarization effects. PhosO nanoflakes turn convenient to recycle via simple treatment with alkaline eluents because these show a strong repulsive surface at high pH. Indeed, PhosO makes easier the regeneration with alkaline eluents, increasing by ~20% the affinity with hydroxide anions compared with intrinsic phosphorene. Conceptually understanding the adsorption properties of phosphorene oxide towards hazardous methylarsenicals provides a valuable framework for new developments in future water treatment technologies with adsorbents of large surface area, high adsorption capacity/selectivity without requiring pre-oxidation processes, and easy recovery.

Keywords: Environmental pollution; water pollution; surface science; nanotechnology; DFT calculations; adsorption.

1. Introduction

Arsenic (As) is a toxic and highly mobile contaminant, which forms dangerous water-soluble compounds for human health[1,2]. Anthropogenic sources and aquatic organisms allow the methylation of inorganic arsenicals to monomethylated (MMA), dimethylated (DMA), and trimethylated (TMA) arsenic species[3], which usually have a lesser extent than inorganic ones; however, increasing herbicides and pesticides worldwide makes them a dangerous water and groundwater pollutant (Scheme 1a for molecular structures). Moreover, trivalent and pentavalent methylarsenicals promote diabetes *via* distortion of glucose metabolism[4–6]. Due to the latter, the World Health Organization (WHO) has adopted regulatory standards to limit the arsenic concentration in drinking water, imposing a limit value of 10 μg/L[2]. Additionally, the toxicity of methylarsenicals depends on their methylation degree and pH [7]; pentavalent TMA^{V}, $MMA^{V,}$ and DMA^{V} species are less toxic than inorganic pentavalent arsenicals (iAs^{V}); while the trivalent MMA^{III}, $DMA^{III,}$ and TMA^{III} species are much more toxic than inorganic trivalent forms (iAs^{III}). Thus, the toxicity depends on the uptake rate of each arsenic compound where less toxic species (pentavalent forms) can be converted to the more toxic species (trivalent forms) increasing in the following order; $TMA^{V} < MMA^{V} \approx DMA^{V} < iAs^{V} < < iAs^{III} < MMA^{III} < DMA^{III} < TMA^{III}$[8,9].

In this regard, two-dimensional 2D materials are a useful alternative for drinking water treatment via physical/chemical adsorption of arsenic pollutants, favored by their high surface area, high adsorption capacity, and high recovery and reusability[10,11]. As an illustration, activated carbons and graphene-based materials have been demonstrated as potential materials for arsenic removal removing with a high adsorptive capacity for a large number of compounds (Scheme 1b-c)[12,13,22–24,14–21], where the hydrophobicity,

recyclability, and adsorption capacity of nanostructured intrinsic surfaces can be remarkably enhanced by surface treatments and oxidation process[25].

Phosphorene-based materials are structurally flexible layers where each phosphorus atom is covalently bonded to three adjacent atoms (Scheme 1d), which have been considered promising candidates in pollutant control technologies. Contrary to graphene, the unique structure of phosphorene allows a direct bandgap of ~1.5 eV, which confers high carrier mobility, and interesting optical and electronic anisotropy[26–28]. Regarding its sorbent ability, phosphorene has already been demonstrated by both theoretical and experimental

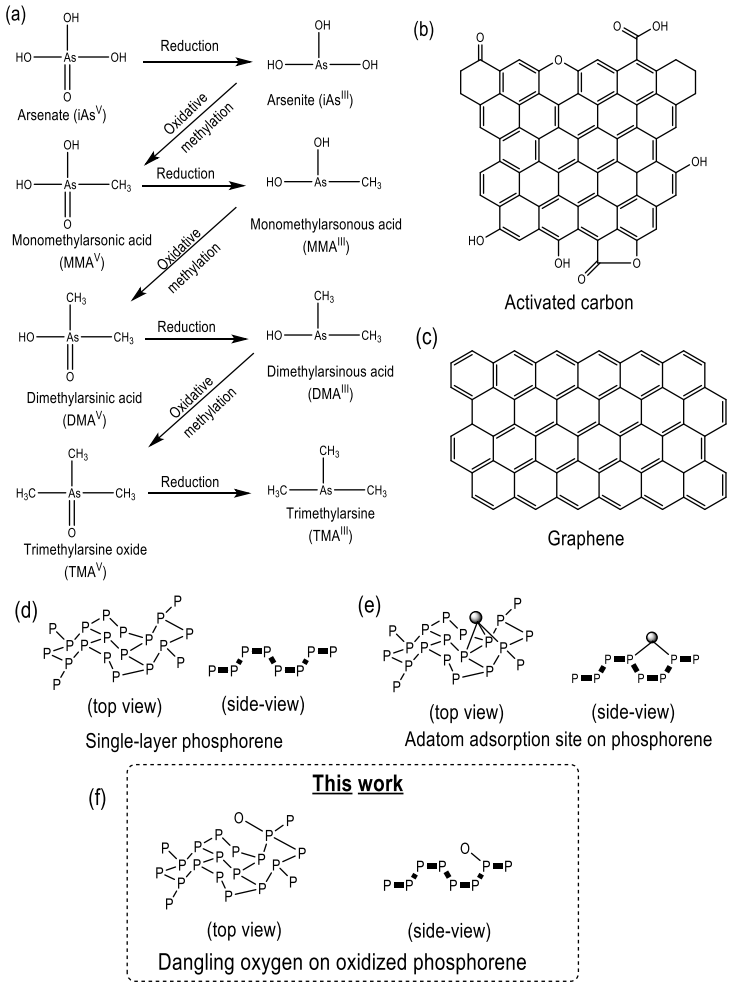

Scheme 1. (a) Structure of methylarsenicals and metabolic pathways for arsenic methylation. (b-f) Low-dimensional adsorbent materials.

investigations a larger adsorption capacity for other aqueous pollutants such as toxic dyes; methylene blue, rhodamine B, and N-nitrosodimethylamine since the strength of binding is highly dependent on the amount of charge transfer between the contaminants and the phosphorene layer, which is characteristic of their electrical resistivity[29,30]. In addition, phosphorene reaches 50-90% efficiency by chemisorption of inorganic arsenicals in water treatment[31]. At the same time, phosphorene shows an adsorption capacity of ~4.8 mg g^{-1} for inorganic iAs^{III} in contrast to graphene, which reaches ~1.3 mg g^{-1} at pH=7[31]. The adsorption strength on phosphorene is often stronger than graphene because the chemically active phosphorous atom makes it have stronger affinity interaction with the atoms or molecules[32]. Additionally, density functional theory (DFT) calculations show that phosphorene doping with transition metals (e.g., Fe, Ni, and Cu, Scheme 1e) enhances the adsorption capacity by a strong inner-sphere surface complexation of chemical nature reaching adsorption energies of up to ~2.0 eV[33,34]. Also, the adsorption efficiency for inorganic arsenic removal remains at acidic and neutral environments, with a low competition of adsorption sites with coexisting species and high reusability/recovery of adsorbents by alkaline treatment[33,34].

On the other hand, it is well known that phosphorene is prone to oxidize when it is exposed to air and water, which changes its structure and properties depending on the type of the formed oxide [P_xO_y or $P_xO_y(OH)_z$][35,36]. A computational study explored many possible reaction products between phosphorene and oxygen, resulting in the most stable species in contact with water, the P_xO type suboxides (with x=8, 6, 4, 2)[37]. This partial oxidation type of phosphorene surface is another interesting property to explore the adsorption ability of this material, which could show an improved adsorption capacity

compared to its pristine counterpart like graphene oxide [38]. The latter turns into a key point because the oxidized forms could be the reliable structures to act as adsorbents in pollutant removal. With this in mind, a surface structure with dangling oxygen atoms (P-O) is the most stable configuration of oxidized phosphorene for low/medium oxygen concentrations (Scheme 1f)[39]. In addition, an easy bottom-up synthesis route for partially oxidized phosphorene surfaces can be addressed[38]. In this way, the properties of pristine phosphorene could be preserved in the oxidized forms, with slight changes in the structure of oxidized phosphorene confirming the primary role of oxygen on the surface and their beneficial application in an aqueous environment[38].

Our motivation is to clarify the role of partially oxidized phosphorene to control water-soluble methylarsenicals, which to our knowledge, has not yet been explored. In particular, the present work addresses a DFT study for (i) the adsorption ability of phosphorene for uptake of methylated As^{III} and As^{V} species in water environments, (ii) adsorption conformations, (iii) the interaction mechanisms and nature of the physical or chemical adsorption, and (v) recovery of the adsorbent material as a new technology for water treatment.

2. Computational Details

We employed all-electron DFT calculations at the PBE/def2-SVP level of theory[40,41]. Dispersion corrections due to van der Waals interactions were included with the DFT-D3(BJ) method[42,43]. Solvent effects in water (ε=80.4) were comprised by the conductor-like polarizable continuum model (CPCM), where the solvent reaction field is described by apparent polarization charges on a cavity surface where the solute is placed[44].

Convergence tolerance values of 1×10^{-8} and 3×10^{-5} Ha were used for energies and geometry optimizations; the geometries were converged with tolerance values in gradients and coordinate displacements of 2×10^{-3} Ha/Bohr and 1×10^{-2} Bohr, respectively. Phosphorene (Phos, $P_{126}H_{30}$) and phosphorene oxide (PhosO, $P_{126}O_{12}H_{30}$) nanoadsorbents were modeled as finite clusters with a surface area of 1583-1611 $Å^2$ (considering its electron density), which is larger compared to methylarsenicals (115-135 $Å^2$). Then, the 126-phosphorous atoms finite model has already been validated to obtain well-converged adsorption energies for arsenical removal[33]. Dangling bonds at the edges are saturated with hydrogen atoms to avoid vacant orbitals[33,34]. According to previous results, the phosphorene oxide was modeled using the 25% oxygen atoms in the structure[45,46]. PhosO with 25% of oxygen content displays the following advantages: (i) the higher stability based on indirect and direct band gaps[45]; (ii) it conserves the phosphorene skeletal structure after active surface oxidation; (iii) the active surface contains equal oxygen and phosphorous atoms as electron donor and acceptor sites, respectively; (iv) a medium content of oxygen atoms reduces the repulsion between negatively charged oxygen atoms and anionic methylarsenicals. The computed cohesive energies are 3.36 and 3.42 eV/atom for Phos and PhosO, denoting the geometrical and energetic stability of the proposed systems.

Adsorption energies (E_{ads}) of the adsorbent-pollutant systems were computed as:

$$E_{ads}=E_{Phos}+E_{as}-E_{phos\text{-}As} \quad \text{(Eq. 1)}$$

where E_{Phos}, E_{As}, and $E_{Phos\text{-}As}$ are the total energies of the free phosphorene-based nanoadsorbent, free arsenic contaminant, and adsorbent-adsorbate system, respectively; then, the more positive the E_{ads} values, the more stable the adsorption is. The standard counterpoise

correction was used to avoid basis set superposition errors[47]. Adsorption energies in water were further decomposed into physically meaningful terms for quantitative characterization of the adsorption mechanism *via* the energy decomposition analysis based on absolutely localized molecular orbitals (ALMO-EDA) in the Q-Chem5.2 program[48–51]. Accordingly, the adsorption energy is expressed as the sum of six physical terms:

$$-E_{ads}=\Delta E_{ELEC}+\Delta E_{DISP}+\Delta E_{POL}+\Delta E_{CT}+\Delta E_{PAULI}+\Delta E_{PREP} \quad \text{(Eq. 2)}$$

Here, ΔE_{ELEC}, ΔE_{DISP}, ΔE_{POL}, and ΔE_{CT} are related to the stabilizing energy contributions due to Coulombic attractions (classical intermolecular electrostatic), dispersion forces (van der Waals interactions), polarization (induced electrostatic effects), and charge transfer (inter and intramolecular charge flow between fragments), respectively. ΔE_{PAULI} is the energy destabilization due to Pauli repulsion when two fragments are close enough (volume exclusion effects). ΔE_{PREP} is the preparation energy due to geometric/electronic distortion of the fragments to reach the geometry of the adsorbent-adsorbate system.

We employed the Atoms-in-Molecules (AIM) method to demonstrate the fingerprint of chemical interactions, which quantifies the electron density (ρ_i) at the bond critical points (BCPs) of intermolecular interactions[52]. In this framework, covalent bonds, coordinate covalent bonds and hydrogen bonds (highly polarized interactions), and weak electrostatic interactions show ρ_i values of ~0.50−0.10, 0.10-0.04 ≤0.01 e/Bohr^3, respectively. AIM, Mayer bond orders, Mulliken population analyses, and wavefunction analyses were performed in the Multiwfn 3.7 program[53]. An orbital picture of the bonding was obtained through the natural bond orbital NBO module in Gaussian16 at the same level of theory[54].

3. Results and Discussion

In terms of toxicity, trivalent arsenicals are more toxic and mobile than pentavalent ones, which is related to the speciation and its affinity with the -SH groups in biomolecules such as glutathione and cysteinyl residues in enzymes[55–57]. In the first place, trivalent arsenicals are deprotonated above pH=9.2; then, trivalent arsenicals are neutrally charged at neutral and physiological pH[55,58]. Besides, pentavalent methylarsenicals show acid-base equilibria in solution:

$$MMA^{V} \rightleftharpoons H^{+} + aMMA^{V},\ pKa_1=4.1 \quad \text{(Eq. 3)}$$

$$aMMA^{V} \rightleftharpoons H^{+} + CH_3AsO_3^{2-},\ pKa_2=8.7 \quad \text{(Eq. 4)}$$

$$DMA^{V} \rightleftharpoons H^{+} + aDMA^{V},\ pKa_1=6.2 \quad \text{(Eq. 5)}$$

According to Eq. 3-5, pentavalent methylarsenicals are anionic at pH=7, while TMA^{V} is non-protic. Given these points, the adsorption ability of oxidized phosphorene is evaluated by the adsorption energies E_{ads} (Fig. 1), where positive values indicate a stable adsorption.

3.1. Interaction stability

Firstly, the stability of the arsenicals adsorbed onto Phos and PhosO were studied using adsorption energy in water (E_{ads}, Fig. 1). To have a comparative perspective, the adsorption onto intrinsic phosphorene is contemplated. Neutral trivalent and pentavalent methylarsenicals show adsorption energies onto intrinsic phosphorene in the range of 0.35-0.68 eV, while anionic pentavalent methylarsenicals shows adsorption energies of up to 1.33 eV. On the side of phosphorene oxide, the neutral methylarsenicals display adsorption

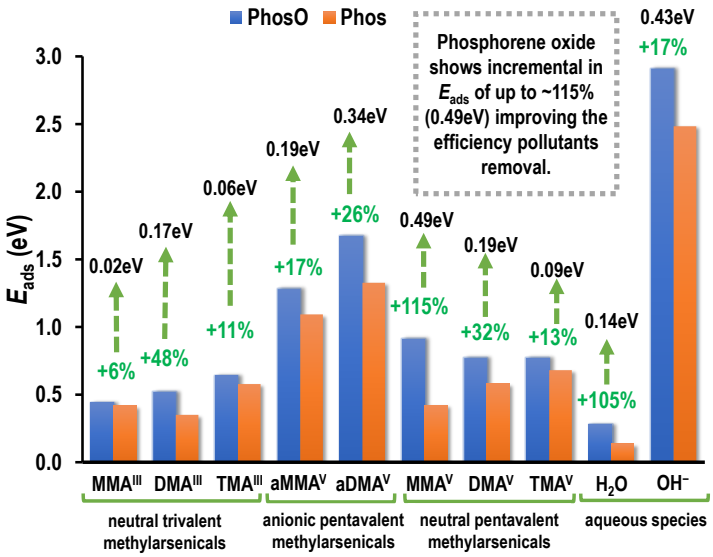

Fig. 1. Adsorption energy of adsorbed methylarsenicals and aqueous species. Values in black are the adsorption energy difference with respect to intrinsic phosphorene [$\Delta E_{ads}=E_{ads}$(PhosO)$-E_{ads}$(Phos)]; values in green are the respective percentual increase.

energies between 0.42 and 0.91 eV, reaching an increment of up to 0.49 eV compared to intrinsic phosphorene. Anionic pentavalent methylarsenicals reach adsorption energies of 1.28-1.67 eV on phosphorene oxide, increasing up to 0.34 eV compared to intrinsic material. These results illustrate the positive effect on the stabilization of methylarsenicals onto phosphorene oxide as nanoadsorbent.

3.1.1. Adsorption of trivalent methylarsenicals

Two main conformations were found for methylarsenicals onto Phos and PhosO nanoadsorbents (Fig. 2): (i) *lying-down*, where the substituents (CH_3 and OH) are oriented towards the adsorbent surface (Fig. 2a,b,d); (ii) *standing*, where the As atom confronts straightforward to the adsorbent surface (Fig. 2c,e,f). In the cases of methylarsenicals absorbed onto intrinsic phosphorene, *lying-down* conformations were obtained for MMA^{III} and DMA^{III}, but a *standing* conformation for TMA^{III}; these systems show intermolecular bond lengths on the range of $d_{Phos\text{-}As}$=2.8-4.1 Å and adsorption energy of up to 0.58 eV. In

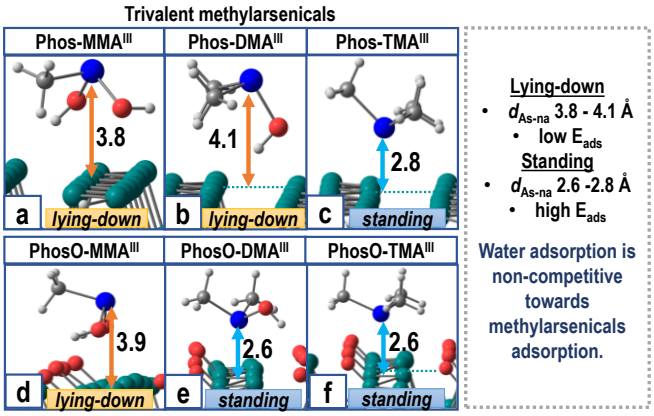

Fig. 2. Trivalent methylarsenicals adsorbed onto Phos (a-c) and PhosO (e-f) nanoadsorbents. As-adsorbent distances are displayed in Å.

the case of phosphorene oxide, the standing conformation is adopted by DMA^{III} and TMA^{III}, ($d_{PhosO-As}$=2.6 Å), with adsorption energies of 0.52-0.64 eV, respectively, which overcome the stabilization by MMA^{III} (E_{ads}=0.44 eV). To summarizing, *lying-down* complexes are less stable than *standing* complexes. Noteworthy methylarsenicals adsorbed onto PhosO are always thermodynamically favored, presenting an adsorption energy difference with respect to intrinsic phosphorene difference [$\Delta E_{ads}=E_{ads}$(PhosO) – E_{ads}(Phos)] with positive values that reach up to 0.17 eV for DMA^{III} (Fig. 1, values in black). Thus, the ΔE_{ads} values oscillate between ~5% and ~50%, demonstrating the improvement of adsorption properties of PhosO compared with intrinsic phosphorene. For comparison, the adsorption of trivalent methylarsenicals onto intrinsic bidimensional materials such as graphene is less efficient in an aqueous environment due to lower adsorption energies (E_{ads}≈0.3 eV[16]) compared with intrinsic phosphorene and phosphorene oxide (E_{ads}≈0.5 eV, this work).

Literature cases offer a comparative landscape of these results since are reached adsorption energies of 0.5 to 1.5 eV, in the case of iAs^{III} neutral species interacting with Phos and Ni/Cu-doped phosphorene, respectively [34]. Another theoretical study considering

202 iAs^{III} and methylated As^{III} adsorbed onto doped Fe/Al-doped graphene reaches adsorption
203 energies of 1.7 eV[16]; the adsorption mechanism is mainly related to monodentate
204 complexation of the pollutant due to bond formation between oxygen and the doping metal.
205 Fe-doped phosphorene also interacts with iAs^{III} species, displaying E_{ads} values between 1.1
206 and 2.0 eV, where a bidentate complex is observed for the most stable conformation[33]. For
207 graphene and carbonyl-functionalized graphene, the adsorption of iAs^{III} reaches adsorption
208 energies of 0.3 and 0.5 eV[59]; these results reflect the improvement of the stabilization and
209 the effectiveness for the arsenical removal oxidating the adsorbent surface.

210 **3.1.2. Adsorption of pentavalent methylarsenicals**

211 Two conformations were obtained for adsorbed pentavalent methylarsenicals
212 according to their speciation at neutral pH (Fig. 3): (i) *lying-down* or (ii) *seated*
213 conformations, where deprotonated oxygen of methylarsenicals is oriented toward the
214 adsorbent surface, while the arsenic atom is placed at intermolecular distances of 3.0-3.7 Å
215 from the adsorbent surface. In comparison, neutral pentavalent methylarsenicals reach
216 adsorption energies of 0.42-0.68 eV onto intrinsic phosphorene. In the case of pentavalent
217 methylarsenicals adsorbed onto phosphorene oxide, a slight shortening of intermolecular
218 length ($d_{PhosO\text{-}As}$) is accompanied to an increase of stabilization compared to the intrinsic
219 phosphorene; that is, neutral pentavalent methylarsenicals display E_{ads} of 0.77-0.91 eV
220 showing a substantial increment of up to 115% (+0.49 eV) in the adsorption process for
221 MMA^{V} (Fig. 1). Concerning the adsorption of anionic pentavalent methylarsenicals, the
222 adsorption process is substantially more robust using phosphorene oxides as nanoadsorbents.
223 For instance, the adsorption energy reaches 1.67 eV for PhosO–$aDMA^{V}$, displaying the
224 stronger adsorption. Geometrical differences are observed in the participation of methyl

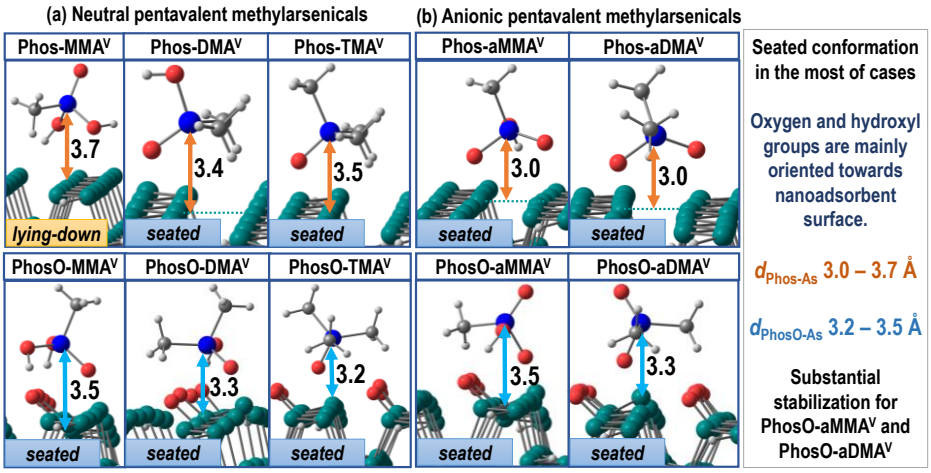

Fig. 3. Molecular structures of (a) neutral pentavalent methylarsenicals and (b) anionic pentavalent methylarsenicals adsorbed onto Phos and PhosO nanoadsorbents. Lengths from As atom to the phosphorene-based structure are displayed in Å.

groups pointing to the oxygen atoms of PhosO while one deprotonated oxygen is towards the surface phosphorous atoms (Fig. 3b). According to literature, the adsorption of iAs^V, MMAs^V, and DMAs^V onto pristine graphene reaches adsorption energies of ~0.5-0.7 eV, while higher values are reached with metal-doped graphene (~2.9-4.2 eV)[16]. Besides, iAs^V and DMA^V adsorbed onto hematite rise E_{ads} of 0.60 and 0.34 eV, respectively, where a non-complexation process via hydrogen bonding is verified by ATR-FTIR spectroscopy [60].

From a general perspective, the average adsorption energies for methylarsenicals absorbed onto intrinsic phosphorene and phosphorene oxide (Fig. 4) demonstrate that PhosO is more efficient than intrinsic phosphorene (incremental between ~20 and 46%) for all the studied methylarsenicals, and it is responsible for strong adsorption using phosphorene in water. An increase in arsenical removal efficiency was observed for As(III) removal for graphene/graphene oxide[59]. Therefore, the controlled incorporation of oxygen atoms on phosphorene surfaces offers an exciting route to improve the efficiency of removing methylarsenicals pollutants.

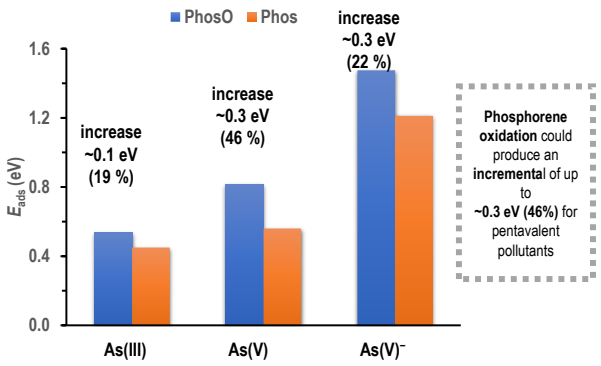

Fig. 4. Comparative average adsorption energy (E_{ads}) for trivalent and pentavalent methylarsenicals adsorbed onto intrinsic phosphorene and phosphorene oxide.

3.2. Energy Decomposition Analysis.

The adsorption energies of the inner-sphere surface complexes were decomposed for a quantitative and readily physical interpretation of interaction mechanisms. According to the ALMO-EDA method, we focused the attention on the stabilizing terms of Eq. (2) (ΔE_{ELEC}, ΔE_{DISP}, ΔE_{POL}, ΔE_{CT}). Their relative single contributions (in percentage) are displayed in Fig. 5 for a standardized comparison. Energies are included in Table S1.

Regarding neutral trivalent methylarsenicals, the adsorption energy is strongly determined by the magnitude of intermolecular electrostatic interactions, with an ΔE_{ELEC} contribution of up to 61% (Fig. 5a). Note that ΔE_{ELEC} in aqueous solution also tracks the energy penalty due to the solvation process because Coulomb potential V is inversely proportional to the solvent dielectric constant (ε); in other words, ΔE_{ELEC} contains the contribution from solvation energies. With this in mind, electrostatic interactions are a key stabilizing driving force even in aqueous environments. Despite the latter, the charge-transfer term (ΔE_{CT}) displays the second-highest contribution (up to 38%), in agreement with the

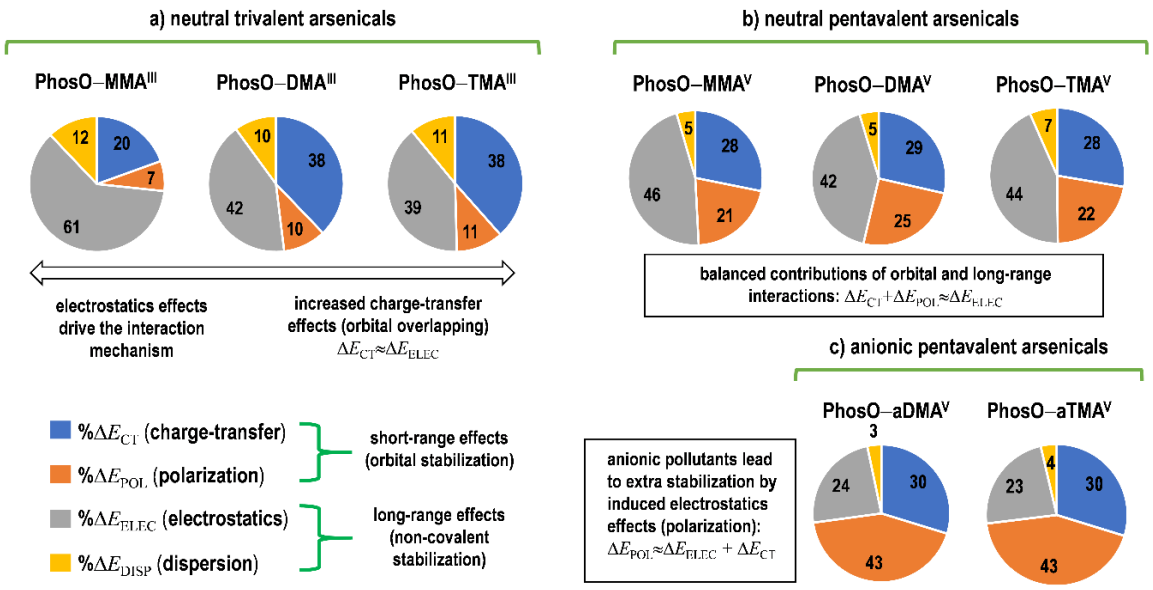

Fig. 5. Relative single percentage contributions of EDA terms to the stabilizing energy of adsorbed methylarsenicals: a) neutral trivalent, b) neutral pentavalent, c) anionic pentavalent.

253 relative high magnitude of electron transfer between methylarsenicals and phosphorene oxide
254 (pollutants transfer ~0.2–0.4 electrons after uptake, indicating its donor character or pollutant
255 → PhosO electron transfer). Thus, the key stabilization gained by ΔE_{CT} contribution is related
256 to the charge-flow between fragments upon adsorption, i.e., increasing the number of methyl
257 groups increases in methylarsenicals. In addition, the larger magnitude of ΔE_{CT} term in the
258 case of PhosO–DMA^{III} and PhosO–TMA^{III} complexes explain their relatively higher
259 adsorption energies than the MMA^{III} adsorption, mainly because ΔE_{CT} term show
260 dependence on orbital interactions, relative orientation, and separation between molecular
261 fragments. Therefore, the arsenic atom of DMA^{III} and TMA^{III} must be influenced by the
262 substrate at shorter intermolecular distances. As an illustration, the PhosO–MMA^{III} complex
263 ($d_{PhosO-As} \approx 3.9$ Å) shows a higher ΔE_{CT}=-0.79 eV than PhosO–DMA^{III} complex ($d_{PhosO-As} \approx 2.6$
264 Å) with ΔE_{CT}=-2.41 eV. In particular, ΔE_{CT} is associated with orbital interactions at short-
265 range distances, denoting orbital overlapping in the PhosO–DMA^{III} and PhosO–TMA^{III}

complexes, which agrees with their relative higher values of electron transfer. As can be seen, the inner-sphere surface adsorption mechanism of trivalent methylarsenicals is driven by electrostatic forces and contributed from charge-transfer (orbital) stabilization, standing for a combined contribution of ~80%. With this in mind, we cannot assume hydrogen bonding as the primary interaction mechanism from the structural motif, revealing the relevance of our energy decomposition analyses. Otherwise, dispersion forces (ΔE_{DISP}) have a minor contribution (10-12%), comparable to polarization effects (7-11%). As a comparison, the As(III) physisorption onto intrinsic phosphorene is 28% due to dispersion energies, implying the different way as arsenicals are stabilized onto phosphorene oxide[33,34].

In the case of pentavalent methylarsenicals, some interesting mechanistic features emerge because of the oxide groups and charge speciation. For neutral pollutants, the combined contribution from charge transfer and polarization effects ($\Delta E_{CT}+\Delta E_{POL}$) accounts for up to 54% of the stabilizing energy, which is almost balanced with the electrostatic term (ΔE_{ELEC}, 42-46%, Fig. 5b). Because ΔE_{CT} and ΔE_{POL} show a strong dependence of orbitals interactions at shorter intermolecular distances, oxide groups of pentavalent methylarsenicals must covalently bind with activated phosphorous atoms of the adsorbent, in agreement with short O–P bonds in neutral PhosO–As^{V} complexes ($d_{O-P}\approx1.8$ Å). Consequently, the inner-sphere surface complexation of pentavalent methylarsenicals occurs by a balanced contribution of orbital and long-range driving forces, explaining their relatively higher adsorption energies than trivalent pollutants. Note that the oxide group of pentavalent pollutants is also responsible for strong chemical bonding onto doped substrates like Al, Fe, and Si-doped graphene, denoting its key role in the low mobility of As(V) species compared to As(III) [14,16].

On the other hand, anionic pentavalent arsenicals show a high stabilization *via* polarization effects, with a relative ΔE_{POL} contribution of 43% (Fig. 5c). According to their speciation, $aMMA^{V}$ and $aDMA^{V}$ are found with a negative charge at the removal pH due to their acid-base equilibria (Eq. 3-5); the negative charge of adsorbates induces strong polarization in the phosphorene oxide nanoadsorbents, leading to the on-fragment relaxation of each species to the presence of their nuclei and electrons. The on-fragment relaxation comes in the form of electron density rearrangements that create favorably aligned induced multipole moments, favoring the energy lowering. Consequently, the anionic charge of pentavalent species ensures higher adsorption energies and lower mobility compared to the uptake of neutral pollutants. Note that part of the polarization stabilization also comes from the covalent O–P bonding, but charge transfer effects are almost balanced with electrostatics effects in these complexes (combined $\Delta E_{CT}+\Delta E_{ELEC}$ contribution of 53-54%). Finally, dispersion forces show a negligible contribution to the stability of anionic/neutral pentavalent methylarsenicals (ΔE_{DISP}, up to 7%).

Last but not less, Pauli repulsion (ΔE_{PAULI}) compensates for all the stabilizing effects, standing for 84-97% of the whole destabilizing energy. Pauli repulsion is related to the volume exclusion effects when molecular fragments are brought into close interaction. Due to the latter, ΔE_{PAULI} is sensitive to the number of methyl groups, molecular volume, oxidation state, and relative adsorption orientation in methylarsenicals. For instance, ΔE_{PAULI} is higher for anionic PhosO–$aMMA^{V}$ complex ($\Delta E_{PAULI}\approx11.8$ eV) compared to neutral PhosO–MMA^{III} ($\Delta E_{PAULI}\approx3.4$ eV), which is due to the anionic nature, relatively higher molecular volume, and short-range P–O bonding in the pentavalent case (Table S1).

3.3. Characteristics of chemical bonding.

EDA results revealed the key contribution of orbital interactions to the adsorption stability. We performed electron density-based analyses to address the chemical fingerprint of the surface complexation. We evaluate the electron density values (ρ_i) at the intermolecular bond critical points [BCPs, points in space at which the first derivatives of the electron density vanish $\nabla\rho(r)=0$]. First, the non-covalent part of the PhosO–Pollutant bonding is associated with strong electrostatic interactions and hydrogen bonding, which are associated to ρ_i values of the order of ~0.06-0.02 *e*/Bohr^3 (red values, Fig. 6), which is a characteristic of electrostatic interactions and supporting the key role of electrostatics interactions as noted by EDA results. Additionally, methyl groups of methylarsenicals accumulate electron density upon adsorption, which electrostatically attracts the electron-deficient atoms of PhosO near the adsorption site. The latter results in several electrostatically attracted pairs with ρ_i values of ~0.02-0.01 *e*/Bohr^3 at BCPs (green values, Fig. 6).

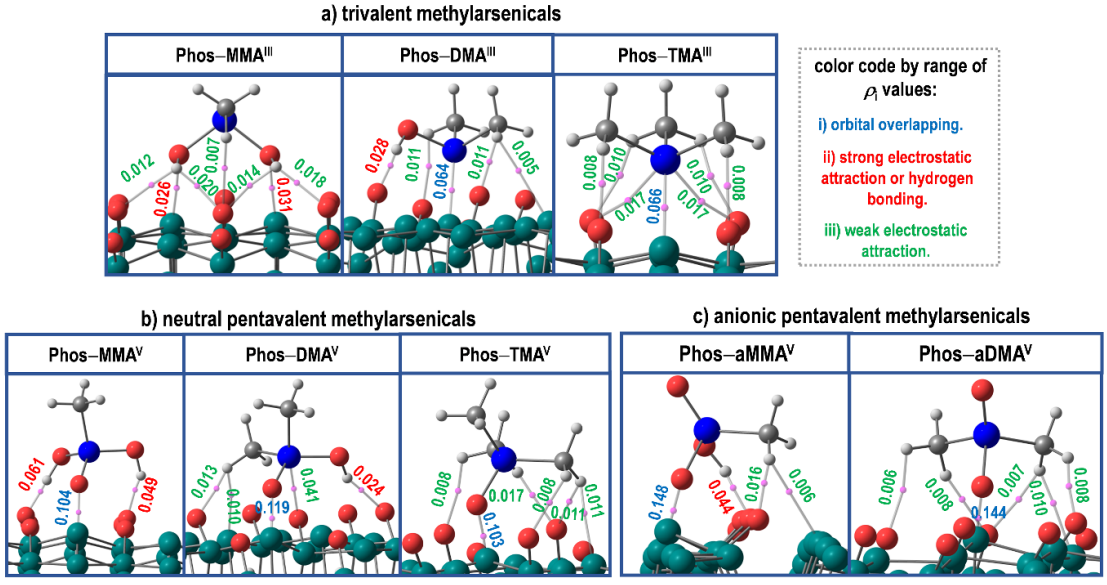

Fig. 6. Electron density at the bond critical points of intermolecular interactions (ρ_i, in *e*/Bohr^3).

In the case of orbital interactions, some differences arise between trivalent and pentavalent methylarsenicals. Orbital interactions increase for trivalent pollutants depending on the adsorption orientation because arsenic atom must be closer to phosphorous atoms. The As–P bonding is associated with ρ_i values of 0.06-0.07 *e*/Bohr^3 in the PhosO–DMA^{III} and PhosO–TMA^{III} complexes as expected for orbital interactions (blue values, Fig. 6a), in agreement with the high ΔE_{CT} contribution in these cases (see section 3.2). The NBO procedure clarifies the orbital picture of the bonding, where PhosO−TMA^{III} and PhosO−TMA^{V} complexes are considered as representative cases. Accordingly, the P–As covalent bond occurs by overlapping of 3*p* (phosphorous) and sp^3 hybridized (arsenic) orbitals, forming one σAs–P covalent bond by sharing one electron pair (Fig. 7a). The bonding density is ~60% polarized to methylarsenicals due to their acceptor character; as a result, the σAs–P bonding strength is lower compared to standard σP–P or σAs–C bonds. In fact, the Mayer bond order for single covalent bonds is ~1.0 a.u., but single σAs–P bonds show bond order of ~0.5 a.u, which is a consequence that σAs–P bonds can delocalize bond density to intramolecular σ*As–C bonds *via* donor-acceptor interactions (electron

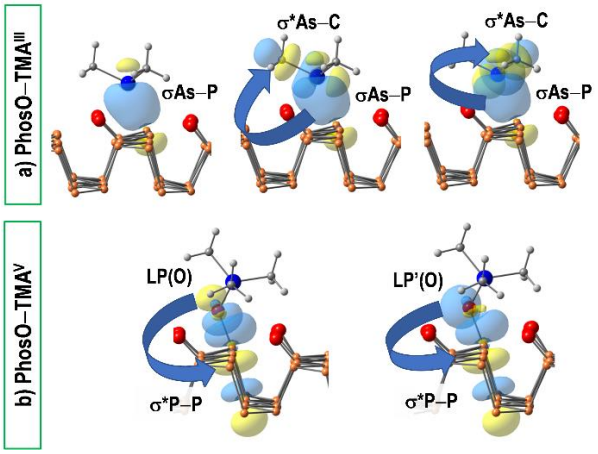

Fig. 7. Natural bond orbitals associated with bonds in the a) PhosO–TMA^{III} and b) PhosO–TMA^{V} complexes. Blue arrows stand for donor-to-acceptor orbital interactions.

delocalization) (blue arrows, Fig. 7a). On the positive side, this bonding behavior balances two main features: i) it allows pollutant desorption in further steps for sorbent recovery; ii) it avoids pollutant decomposition into harmful compounds due to heavy complexation on the surface. Additionally, PhosO–MMA^{III} complex do not show σAs–P bonding, but there is a strong intermolecular O···P attraction due to the low electronegativity of phosphorous atoms compared to oxygen [P (2.19) and O (3.44), in the Pauling scale] (blue values, Fig. 6a).

In the case of pentavalent methylarsenicals, the short orbital O–P interactions ($d_{P–O}$≈1.8 Å) show high ρ_i values of 0.10-0.14 *e*/$Bohr^3$ (blue values, Fig. 6b-c). The O–P interaction is a coordinative covalent bond due to electron delocalization from 2*p* oxygen lone pair orbitals in methylarsenicals toward one low-occupied σ*P–P bond of PhosO (Fig. 7b). Provided that the acceptor antibonding σ*P–P bond is occupied by ~0.3 electrons, destabilizing steric energy must increase in agreement with higher ΔE_{PAULI} energies in the case of adsorbed As(V) species. The O–P bonding features also allow the balance between stable adsorption without pollutant decomposition and desorption ability for further recovery.

3.4 Assisted adsorption by water and recovery

Before exploring the adsorption ability of PhosO nanoadsorbents, it is necessary to analyze the competitiveness of the adsorption site with water molecules. Fig. 1 shows that all arsenic species are more efficiently adsorbed than a water molecule. The water adsorption onto PhosO display lower adsorption energy values than methylarsenicals (E_{ads}≈0.5 eV). Thus, a water molecule is not competitive enough to disrupt the methylarsenicals adsorptions onto oxidized phosphorene. These results agree with the experimental and theoretical evidence, where phosphorene and its derivatives can be employed as effective adsorbents for

arsenical removal from aqueous matrices since pollutants can be adsorbed more strongly than water molecules[31,33,34,61].

In this regard, the superior adsorption ability towards arsenic species is attributed to the orbital part of the bonding, as shown by EDA and bonding results. However, this is not the case for the trivalent monomethyl arsenic TMA^{III}, which is the only physisorbed contaminant since the electrostatic effect is the most prominent interaction with the oxidized phosphorene surface (Table S1), even with a greater adsorption ability than the water molecule. Therefore, these results suggest that phosphorene oxide may not be intrinsically hydrophilic because the water molecule is weakly physisorbed, which makes this material a good candidate for water treatment. This agrees with the findings of the Sutter group[62]; they found that water adsorption does not perceptibly change the structure of oxidized phosphorene, confirming the primary role of oxygen on the surface in front of the water.

In an explicit water environment (Fig. 8), the physisorption mechanism prevails for MMA^{III} because electron densities at the BCP of intermolecular interactions are in the range of ~0.02-0.01 e/Bohr^3, which is related to electrostatic interactions. A similar trend is observed for the anionic DMA^{V} forms (Fig. 8a), where the chemisorption prevails, as noted from the high electron density values at the BCP of P–O bond (ρ_i=0.113 e/Bohr^3) with a slight change related to the implicit solvent model (ρ_i=0.144 e/Bohr^3). Consequently, only the monomethylated trivalent species of arsenic will have relatively higher mobility than the rest of the methylarsenicals. Thus, it could be predicted that the mobility in water decreases accordingly to the electron densities at the BCP in the following order: MMA^{III}<DMA^{III}<TMA^{III}<TMA^{V}<MMA^{V}<DMA^{V}<aDMA^{V}<aMMA^{V}.

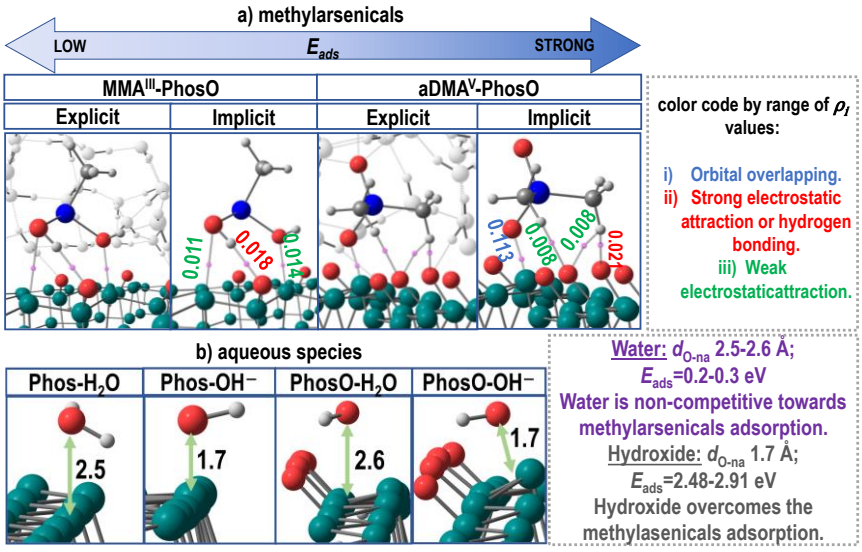

Fig. 8. PhosO–MMA^{III} and PhosO–aDMA^{V} systems at water environments (hydrogen bonds of water molecules are depicted with white points). Numbers stand for ρ_I values at the BCPs of intermolecular interactions in *e*/Bohr^3. (b) Molecular structures of single H_2O and OH^- species adsorbed onto Phos and PhosO, with distances in Å.

Water molecules demonstrate lower adsorption energies for adsorption on either intrinsic or oxidized phosphorene (E_{ads} 0.14 and 0.28 eV for Phos–H_2O and PhosO–H_2O, respectively), adopting an intermolecular distance from oxygen to nanoadsorbent of 2.5-2.6 Å (Fig. 8b). The adsorption energy of water onto intrinsic phosphorene or phosphorene oxide is always lower (at least 40%) than methylarsenicals adsorption, showing the selectivity of methylarsenicals to be absorbed in aqueous environments. In this sense, water molecules are non-competitive factors for arsenic remotion with phosphorene-based nanoadsorbent.

Water treatment technology looks for sorbent materials capable of resisting several adsorption-desorption cycles for repetitive use. For regeneration and reusability of nanoadsorbents, surface treatment with alkaline eluents (e.g., NaOH solutions) allowed the regenerations by removing the ~99% of arsenic from graphene-oxide composites with metal oxides such as $CuFe_2O_4$, Gd_2O_3, Fe_3O_4, and CuO), Zn-Fe mixed metal oxides,

Fe_3O_4/Halloysite nanocomposites, Fe/Cu-polyurethane nanoparticles, and Ti-oxides[63–66]. Hence, the reusability was investigated considering the hydroxide anion (OH^-) adsorption as eluent. Fig. 1 shows that the hydroxide anion (OH^-) competitiveness with the arsenic species is much higher (E_{ads}=2.91 eV) given its strong stabilization by polarization effects with phosphorene oxide (see Table S1) and displaying an intermolecular length of 1.7 Å. The latter prevents the adsorption of arsenic species by repulsive electrostatic interactions with the adsorbent surface in alkaline conditions. Additionally, the results indicate that phosphorene oxide makes easier the regeneration with alkaline eluents increasing the stabilization by ~20% compared with the affinity of intrinsic phosphorene with hydroxide anions. In other words, the regeneration of adsorbent is allowed by inexpensive alkaline reagents such as sodium hydroxide solution, i.e., through suitable modifications operating settings, such as pH conditions. In addition, also it has been demonstrated that a 1,2-ethanedithiol (EDT) treatment is a simple and effective way to completely recovered even to its pristine state[67]. Similarly, another method for recovering nanoadsorbents has been rinsing with deionized water and following with post-treatment[68].

4. Conclusions

In summary, we have elucidated the ability of oxidized phosphorene nanoflakes (PhosO) for the simultaneous removal of methylarsenicals from contaminated water sources. The PhosO nanoflakes form inner-sphere surface complexes with methylarsenicals under water conditions, even with enhanced adsorption stability compared to intrinsic phosphorene and without the competition of water molecules for adsorption sites. The inner-sphere surface adsorption of trivalent methylarsenicals is driven by electrostatic forces and contributed from charge-transfer (orbital) stabilization. While surface complexation of pentavalent methylarsenicals occurs by a balanced

contribution of orbital and long-range driving forces, allowing relative higher adsorption energies than trivalent pollutants; anionic contaminants also show a high stabilization via extra polarization effects. Furthermore, recovery of nanoadsorbent after uptake turns convenient via inexpensive alkaline post-treatments. Therefore, phosphorene oxide could serve as a remarkable basis material for future technologies related to adsorption, removal, and/or control of water-soluble methylarsenicals.

Acknowledgments.

D.C-A thanks the financial support of the ANID/FONDECYT project 11170289 and the computational resources through the ANID/FONDEQUIP project EQM180180. D.E.O. thanks the financial support of ANID+REC CONVOCATORIA NACIONAL SUBVENCIÓN A INSTALACIÓN EN LA ACADEMIA CONVOCATORIA AÑO 2020 +PAI77200068. K.W-A acknowledges the financial support of ANID/FONDECYT Postdoctorado project 3200270. Powered@NLHPC: This research was partially supported by the supercomputing infrastructure of the NLHPC (ECM-02).

References

[1] J.W. Stuckey, M. V. Schaefer, B.D. Kocar, J. Dittmar, J.L. Pacheco, S.G. Benner, S. Fendorf, Peat formation concentrates arsenic within sediment deposits of the Mekong Delta, Geochim. Cosmochim. Acta. 149 (2015) 190–205. https://doi.org/10.1016/j.gca.2014.10.021.

[2] World Health Organization, Arsenic, (n.d.). http://www.who.int/ipcs/assessment/public_health/arsenic/en/.

[3] O. Thirunavukkarasu, T. Viraraghavan, K. Subramanian, S. Tanjore, Organic arsenic removal from drinking water, Urban Water. 4 (2002) 415–421. https://doi.org/10.1016/S1462-0758(02)00029-8.

[4] I. Khairul, Q.Q. Wang, Y.H. Jiang, C. Wang, H. Naranmandura, Metabolism, toxicity and anticancer activities of arsenic compounds, Oncotarget. 8 (2017) 23905–23926. https://doi.org/10.18632/oncotarget.14733.

[5] Y. Kobayashi, T. Agusa, Arsenic Metabolism and Toxicity in Humans and Animals: Racial and Species Differences, in: H. Yamauchi, G. Sun (Eds.), Springer Singapore, Singapore, 2019: pp. 13–28. https://doi.org/10.1007/978-981-13-2565-6_2.
[6] M. Ozturk, M. Metin, V. Altay, R.A. Bhat, M. Ejaz, A. Gul, B.T. Unal, M. Hasanuzzaman, L. Nibir, K. Nahar, A. Bukhari, M.A. Dervash, T. Kawano, Arsenic and Human Health: Genotoxicity, Epigenomic Effects, and Cancer Signaling, Biol. Trace Elem. Res. (2021). https://doi.org/10.1007/s12011-021-02719-w.
[7] P. Smedley, D. Kinniburgh, A review of the source, behaviour and distribution of arsenic in natural waters, Appl. Geochemistry. 17 (2002) 517–568. https://doi.org/10.1016/S0883-2927(02)00018-5.
[8] S. Shankar, U. Shanker, Shikha, Arsenic Contamination of Groundwater: A Review of Sources, Prevalence, Health Risks, and Strategies for Mitigation, Sci. World J. 2014 (2014) 1–18. https://doi.org/10.1155/2014/304524.
[9] T. Watanabe, S. Hirano, Metabolism of arsenic and its toxicological relevance, Arch. Toxicol. 87 (2013) 969–979. https://doi.org/10.1007/s00204-012-0904-5.
[10] A.A. Basheer, New generation nano-adsorbents for the removal of emerging contaminants in water, J. Mol. Liq. 261 (2018) 583–593. https://doi.org/10.1016/j.molliq.2018.04.021.
[11] D. Mohan, C.U. Pittman, Arsenic removal from water/wastewater using adsorbents—A critical review, J. Hazard. Mater. 142 (2007) 1–53. https://doi.org/10.1016/j.jhazmat.2007.01.006.
[12] A. Bhatnagar, W. Hogland, M. Marques, M. Sillanpää, An overview of the modification methods of activated carbon for its water treatment applications, Chem. Eng. J. 219 (2013) 499–511. https://doi.org/10.1016/j.cej.2012.12.038.
[13] J. Rivera-Utrilla, M. Sánchez-Polo, V. Gómez-Serrano, P.M. Álvarez, M.C.M. Alvim-Ferraz, J.M. Dias, Activated carbon modifications to enhance its water treatment applications. An overview, J. Hazard. Mater. 187 (2011) 1–23. https://doi.org/10.1016/j.jhazmat.2011.01.033.
[14] D. Cortés-Arriagada, A. Toro-Labbé, A theoretical investigation of the removal of methylated arsenic pollutants with silicon doped graphene, RSC Adv. 6 (2016) 28500–28511. https://doi.org/10.1039/C6RA03813A.
[15] L. Hao, M. Liu, N. Wang, G. Li, A critical review on arsenic removal from water using iron-based adsorbents, RSC Adv. 8 (2018) 39545–39560. https://doi.org/10.1039/C8RA08512A.
[16] D. Cortés-Arriagada, A. Toro-Labbé, Aluminum and iron doped graphene for adsorption of methylated arsenic pollutants, Appl. Surf. Sci. 386 (2016) 84–95. https://doi.org/10.1016/j.apsusc.2016.05.154.
[17] L.P. Lingamdinne, S. Lee, J.-S. Choi, V.R. Lebaka, V.R.P. Durbaka, J.R. Koduru, Potential of the magnetic hollow sphere nanocomposite (graphene oxide-gadolinium oxide) for arsenic removal from real field water and antimicrobial applications, J. Hazard. Mater. 402 (2021) 123882. https://doi.org/10.1016/j.jhazmat.2020.123882.
[18] M. Srivastava, A. Srivastava, Cu decorated functionalized graphene for Arsenic sensing in water: A first principles analysis, Appl. Surf. Sci. 560 (2021) 149700. https://doi.org/10.1016/j.apsusc.2021.149700.
[19] S.I. Siddiqui, R. Ravi, S.A. Chaudhry, Removal of Arsenic from Water Using Graphene Oxide Nano-hybrids, in: A New Gener. Mater. Graphene Appl. Water Technol.,

Springer International Publishing, Cham, 2019: pp. 221–237. https://doi.org/10.1007/978-3-319-75484-0_9.
[20] T.K. Das, T.S. Sakthivel, A. Jeyaranjan, S. Seal, A.N. Bezbaruah, Ultra-high arsenic adsorption by graphene oxide iron nanohybrid: Removal mechanisms and potential applications, Chemosphere. 253 (2020) 126702. https://doi.org/10.1016/j.chemosphere.2020.126702.
[21] X. Yang, L. Xia, S. Song, Arsenic adsorption from water using graphene-based materials as adsorbents: A critical review, Surf. Rev. Lett. 24 (2017) 1730001. https://doi.org/10.1142/S0218625X17300015.
[22] H. Su, Z. Ye, N. Hmidi, High-performance iron oxide–graphene oxide nanocomposite adsorbents for arsenic removal, Colloids Surfaces A Physicochem. Eng. Asp. 522 (2017) 161–172. https://doi.org/10.1016/j.colsurfa.2017.02.065.
[23] G.Z. Kyzas, E.A. Deliyanni, K.A. Matis, Graphene oxide and its application as an adsorbent for wastewater treatment, J. Chem. Technol. Biotechnol. 89 (2014) 196–205. https://doi.org/10.1002/jctb.4220.
[24] S.I. Siddiqui, S.A. Chaudhry, A review on graphene oxide and its composites preparation and their use for the removal of $As^{3+}$and As^{5+} from water under the effect of various parameters: Application of isotherm, kinetic and thermodynamics, Process Saf. Environ. Prot. 119 (2018) 138–163. https://doi.org/10.1016/j.psep.2018.07.020.
[25] T.A. Tabish, F.A. Memon, D.E. Gomez, D.W. Horsell, S. Zhang, A facile synthesis of porous graphene for efficient water and wastewater treatment, Sci. Rep. 8 (2018) 1817. https://doi.org/10.1038/s41598-018-19978-8.
[26] F. Xia, H. Wang, Y. Jia, Rediscovering black phosphorus as an anisotropic layered material for optoelectronics and electronics, Nat. Commun. 5 (2014) 4458. https://doi.org/10.1038/ncomms5458.
[27] M. Buscema, D.J. Groenendijk, S.I. Blanter, G.A. Steele, H.S.J. van der Zant, A. Castellanos-Gomez, Fast and Broadband Photoresponse of Few-Layer Black Phosphorus Field-Effect Transistors, Nano Lett. 14 (2014) 3347–3352. https://doi.org/10.1021/nl5008085.
[28] L. Li, Y. Yu, G.J. Ye, Q. Ge, X. Ou, H. Wu, D. Feng, X.H. Chen, Y. Zhang, Black phosphorus field-effect transistors, Nat. Nanotechnol. 9 (2014) 372–377. https://doi.org/10.1038/nnano.2014.35.
[29] J. Wang, Z. Zhang, D. He, H. Yang, D. Jin, J. Qu, Y. Zhang, Comparative Study on the Adsorption Capacities of the Three Black Phosphorus-Based Materials for Methylene Blue in Water, Sustainability. 12 (2020) 8335. https://doi.org/10.3390/su12208335.
[30] V. Nagarajan, R. Chandiramouli, N-nitrosodimethylamine interaction studies on gamma phosphorene sheets emitted from rubber fumes – A first-principles study, Phys. B Condens. Matter. 577 (2020) 411808. https://doi.org/10.1016/j.physb.2019.411808.
[31] O.-P. Chen, Y.-J. Lin, W.-Z. Cao, C.-T. Chang, Arsenic removal with phosphorene and adsorption in solution, Mater. Lett. 190 (2017) 280–282. https://doi.org/10.1016/j.matlet.2017.01.030.
[32] S. Lei, R. Gao, X. Sun, S. Guo, H. Yu, N. Wan, F. Xu, J. Chen, Nitrogen-based gas molecule adsorption of monolayer phosphorene under metal functionalization, Sci. Rep. 9 (2019) 12498. https://doi.org/10.1038/s41598-019-48953-0.
[33] D. Cortés-Arriagada, D.E. Ortega, Removal of arsenic from water using iron-doped phosphorene nanoadsorbents: A theoretical DFT study with solvent effects, J. Mol. Liq. 307 (2020) 112958. https://doi.org/10.1016/j.molliq.2020.112958.

[34] D.E. Ortega, D. Cortés-Arriagada, Exploring the Nature of Interaction and Stability between Water-Soluble Arsenic Pollutants and Metal–Phosphorene Hybrids: A Density Functional Theory Study, J. Phys. Chem. A. 124 (2020) 3662–3671. https://doi.org/10.1021/acs.jpca.0c00532.
[35] M.B. Tahir, N. Fatima, U. Fatima, M. Sagir, A review on the 2D black phosphorus materials for energy applications, Inorg. Chem. Commun. 124 (2021) 108242. https://doi.org/10.1016/j.inoche.2020.108242.
[36] K.L. Kuntz, R.A. Wells, J. Hu, T. Yang, B. Dong, H. Guo, A.H. Woomer, D.L. Druffel, A. Alabanza, D. Tománek, S.C. Warren, Control of Surface and Edge Oxidation on Phosphorene, ACS Appl. Mater. Interfaces. 9 (2017) 9126–9135. https://doi.org/10.1021/acsami.6b16111.
[37] W. Luo, H. Xiang, Two-Dimensional Phosphorus Oxides as Energy and Information Materials, Angew. Chemie Int. Ed. 55 (2016) 8575–8580. https://doi.org/10.1002/anie.201602295.
[38] B. Tian, B. Tian, B. Smith, M.C. Scott, Q. Lei, R. Hua, Y. Tian, Y. Liu, Facile bottom-up synthesis of partially oxidized black phosphorus nanosheets as metal-free photocatalyst for hydrogen evolution, Proc. Natl. Acad. Sci. 115 (2018) 4345–4350. https://doi.org/10.1073/pnas.1800069115.
[39] A. Ziletti, A. Carvalho, D.K. Campbell, D.F. Coker, A.H. Castro Neto, Oxygen Defects in Phosphorene, Phys. Rev. Lett. 114 (2015) 046801. https://doi.org/10.1103/PhysRevLett.114.046801.
[40] J.P. Perdew, K. Burke, M. Ernzerhof, Generalized gradient approximation made simple, Phys. Rev. Lett. 77 (1996) 3865–3868. https://doi.org/10.1103/PhysRevLett.77.3865.
[41] F. Weigend, R. Ahlrichs, Balanced basis sets of split valence, triple zeta valence and quadruple zeta valence quality for H to Rn: Design and assessment of accuracy, Phys. Chem. Chem. Phys. 7 (2005) 3297. https://doi.org/10.1039/b508541a.
[42] S. Grimme, J. Antony, S. Ehrlich, H. Krieg, A consistent and accurate ab initio parametrization of density functional dispersion correction (DFT-D) for the 94 elements H-Pu, J. Chem. Phys. 132 (2010) 154104. https://doi.org/10.1063/1.3382344.
[43] S. Grimme, S. Ehrlich, L. Goerigk, Effect of the damping function in dispersion corrected density functional theory, J. Comput. Chem. 32 (2011) 1456–1465. https://doi.org/10.1002/jcc.21759.
[44] T. Motoba, K. Takahashi, A. Ukhorskiy, M. Gkioulidou, D.G. Mitchell, L.J. Lanzerotti, G.I. Korotova, E.F. Donovan, J.R. Wygant, C.A. Kletzing, W.S. Kurth, J.B. Blake, Link between premidnight second harmonic poloidal waves and auroral undulations: Conjugate observations with a Van Allen Probe spacecraft and a THEMIS all-sky imager, J. Geophys. Res. Sp. Phys. 120 (2015) 1814–1831. https://doi.org/10.1002/2014JA020863.
[45] G. Wang, R. Pandey, S.P. Karna, Phosphorene oxide: stability and electronic properties of a novel two-dimensional material, Nanoscale. 7 (2015) 524–531. https://doi.org/10.1039/C4NR05384B.
[46] A. Ziletti, A. Carvalho, P.E. Trevisanutto, D.K. Campbell, D.F. Coker, A.H. Castro Neto, Phosphorene oxides: Bandgap engineering of phosphorene by oxidation, Phys. Rev. B. 91 (2015) 085407. https://doi.org/10.1103/PhysRevB.91.085407.
[47] S.F. Boys, F. Bernardi, The calculation of small molecular interactions by the differences of separate total energies. Some procedures with reduced errors, Mol. Phys. 19 (1970) 553–566. https://doi.org/10.1080/00268977000101561.

[48] P.R. Horn, Improvements in energy decomposition analysis for single determinant methods, 2015.
[49] P.R. Horn, Y. Mao, M. Head-Gordon, Probing non-covalent interactions with a second generation energy decomposition analysis using absolutely localized molecular orbitals, Phys. Chem. Chem. Phys. 18 (2016) 23067–23079. https://doi.org/10.1039/C6CP03784D.
[50] D.S. Levine, P.R. Horn, Y. Mao, M. Head-Gordon, Variational Energy Decomposition Analysis of Chemical Bonding. 1. Spin-Pure Analysis of Single Bonds, J. Chem. Theory Comput. 12 (2016) 4812–4820. https://doi.org/10.1021/acs.jctc.6b00571.
[51] Y. Shao, Z. Gan, E. Epifanovsky, A.T.B. Gilbert, M. Wormit, J. Kussmann, A.W. Lange, A. Behn, J. Deng, X. Feng, D. Ghosh, M. Goldey, P.R. Horn, L.D. Jacobson, I. Kaliman, R.Z. Khaliullin, T. Kuś, A. Landau, J. Liu, E.I. Proynov, Y.M. Rhee, R.M. Richard, M.A. Rohrdanz, R.P. Steele, E.J. Sundstrom, H.L. Woodcock, P.M. Zimmerman, D. Zuev, B. Albrecht, E. Alguire, B. Austin, G.J.O. Beran, Y.A. Bernard, E. Berquist, K. Brandhorst, K.B. Bravaya, S.T. Brown, D. Casanova, C.-M. Chang, Y. Chen, S.H. Chien, K.D. Closser, D.L. Crittenden, M. Diedenhofen, R.A. DiStasio, H. Do, A.D. Dutoi, R.G. Edgar, S. Fatehi, L. Fusti-Molnar, A. Ghysels, A. Golubeva-Zadorozhnaya, J. Gomes, M.W.D. Hanson-Heine, P.H.P. Harbach, A.W. Hauser, E.G. Hohenstein, Z.C. Holden, T.-C. Jagau, H. Ji, B. Kaduk, K. Khistyaev, J. Kim, J. Kim, R.A. King, P. Klunzinger, D. Kosenkov, T. Kowalczyk, C.M. Krauter, K.U. Lao, A.D. Laurent, K. V. Lawler, S. V. Levchenko, C.Y. Lin, F. Liu, E. Livshits, R.C. Lochan, A. Luenser, P. Manohar, S.F. Manzer, S.-P. Mao, N. Mardirossian, A. V. Marenich, S.A. Maurer, N.J. Mayhall, E. Neuscamman, C.M. Oana, R. Olivares-Amaya, D.P. O'Neill, J.A. Parkhill, T.M. Perrine, R. Peverati, A. Prociuk, D.R. Rehn, E. Rosta, N.J. Russ, S.M. Sharada, S. Sharma, D.W. Small, A. Sodt, T. Stein, D. Stück, Y.-C. Su, A.J.W. Thom, T. Tsuchimochi, V. Vanovschi, L. Vogt, O. Vydrov, T. Wang, M.A. Watson, J. Wenzel, A. White, C.F. Williams, J. Yang, S. Yeganeh, S.R. Yost, Z.-Q. You, I.Y. Zhang, X. Zhang, Y. Zhao, B.R. Brooks, G.K.L. Chan, D.M. Chipman, C.J. Cramer, W.A. Goddard, M.S. Gordon, W.J. Hehre, A. Klamt, H.F. Schaefer, M.W. Schmidt, C.D. Sherrill, D.G. Truhlar, A. Warshel, X. Xu, A. Aspuru-Guzik, R. Baer, A.T. Bell, N.A. Besley, J.-D. Chai, A. Dreuw, B.D. Dunietz, T.R. Furlani, S.R. Gwaltney, C.-P. Hsu, Y. Jung, J. Kong, D.S. Lambrecht, W. Liang, C. Ochsenfeld, V.A. Rassolov, L. V. Slipchenko, J.E. Subotnik, T. Van Voorhis, J.M. Herbert, A.I. Krylov, P.M.W. Gill, M. Head-Gordon, Advances in molecular quantum chemistry contained in the Q-Chem 4 program package, Mol. Phys. 113 (2015) 184–215. https://doi.org/10.1080/00268976.2014.952696.
[52] C.F. Matta, R.J. Boyd, A. Becke, The quantum theory of atoms in molecules: from solid state to DNA and drug design., Wiley-VCH, 2007.
[53] T. Lu, F. Chen, Multiwfn: A multifunctional wavefunction analyzer, J. Comput. Chem. 33 (2012) 580–592. https://doi.org/10.1002/jcc.22885.
[54] M.J. Frisch, G.W. Trucks, H.B. Schlegel, G.E. Scuseria, M.A. Robb, J.R. Cheeseman, G. Scalmani, V. Barone, G.A. Petersson, H. Nakatsuji, X. Li, M. Caricato, A. V. Marenich, J. Bloino, B.G. Janesko, R. Gomperts, B. Mennucci, H.P. Hratchian, J. V. Ortiz, A.F. Izmaylov, J.L. Sonnenberg, D. Williams-Young, F. Ding, F. Lipparini, F. Egidi, J. Goings, B. Peng, A. Petrone, T. Henderson, D. Ranasinghe, V.G. Zakrzewski, J. Gao, N. Rega, G. Zheng, W. Liang, M. Hada, M. Ehara, K. Toyota, R. Fukuda, J. Hasegawa, M. Ishida, T. Nakajima, Y. Honda, O. Kitao, H. Nakai, T. Vreven, K. Throssell, J.A. Montgomery, J.E.P. Jr., F. Ogliaro, M.J. Bearpark, J.J. Heyd, E.N. Brothers, K.N. Kudin, V.N. Staroverov, T.A. Keith, R. Kobayashi, J. Normand, K. Raghavachari, A.P. Rendell, J.C. Burant, S.S. Iyengar,

J. Tomasi, M. Cossi, J.M. Millam, M. Klene, C. Adamo, R. Cammi, J.W. Ochterski, R.L. Martin, K. Morokuma, O. Farkas, J.B. Foresman, D.J. Fox, Gaussian 16, (2016). www.gaussian.com.
[55] V.K. Sharma, M. Sohn, Aquatic arsenic: Toxicity, speciation, transformations, and remediation, Environ. Int. 35 (2009) 743–759. https://doi.org/10.1016/j.envint.2009.01.005.
[56] S. Sharma, M.J. Bezbaruah, I. Ali, M. Choudhury, B. Bezbaruah, Theoretical Investigations on the π-π Stacking Interactions in Phenol-Water Complexes, Comput. Chem. 06 (2018) 15–25. https://doi.org/10.4236/cc.2018.62002.
[57] J. Chen, B.P. Rosen, The Arsenic Methylation Cycle: How Microbial Communities Adapted Methylarsenicals for Use as Weapons in the Continuing War for Dominance, Front. Environ. Sci. 8 (2020) 1–14. https://doi.org/10.3389/fenvs.2020.00043.
[58] K.R. Henke, A. Hutchison, Arsenic Chemistry, in: Arsenic, John Wiley & Sons, Ltd, Chichester, UK, 2009: pp. 9–68. https://doi.org/10.1002/9780470741122.ch2.
[59] D. Cortés-Arriagada, A. Toro-Labbé, Improving As(iii) adsorption on graphene based surfaces: impact of chemical doping, Phys. Chem. Chem. Phys. 17 (2015) 12056–12064. https://doi.org/10.1039/C5CP01313E.
[60] S. Soldoozy, A. Trinh, J.D. Kubicki, H.A. Al-Abadleh, In Situ and Real-Time ATR-FTIR Temperature-Dependent Adsorption Kinetics Coupled with DFT Calculations of Dimethylarsinate and Arsenate on Hematite Nanoparticles, Langmuir. 36 (2020) 4299–4307. https://doi.org/10.1021/acs.langmuir.0c00252.
[61] Y.-J. Lin, W.-Z. Cao, T. Ou Yang, C.-H. Feng, C.-T. Chang, Deciphering the effect of citric acid on arsenic adsorption with phosphorene in aqueous solution, Sustain. Environ. Res. 29 (2019) 22. https://doi.org/10.1186/s42834-019-0021-8.
[62] Y. Huang, J. Qiao, K. He, S. Bliznakov, E. Sutter, X. Chen, D. Luo, F. Meng, D. Su, J. Decker, W. Ji, R.S. Ruoff, P. Sutter, Interaction of Black Phosphorus with Oxygen and Water, Chem. Mater. 28 (2016) 8330–8339. https://doi.org/10.1021/acs.chemmater.6b03592.
[63] Z. Wei, K. Liang, Y. Wu, Y. Zou, J. Zuo, D.C. Arriagada, Z. Pan, G. Hu, The effect of pH on the adsorption of arsenic(III) and arsenic(V) at the TiO_2 anatase [1 0 1] surface, J. Colloid Interface Sci. 462 (2016) 252–259. https://doi.org/10.1016/j.jcis.2015.10.018.
[64] L.-K. Wu, H. Wu, H.-B. Zhang, H.-Z. Cao, G.-Y. Hou, Y.-P. Tang, G.-Q. Zheng, Graphene oxide/$CuFe_2O_4$ foam as an efficient absorbent for arsenic removal from water, Chem. Eng. J. 334 (2018) 1808–1819. https://doi.org/10.1016/j.cej.2017.11.096.
[65] X. Song, L. Zhou, Y. Zhang, P. Chen, Z. Yang, A novel cactus-like Fe_3O_4/Halloysite nanocomposite for arsenite and arsenate removal from water, J. Clean. Prod. 224 (2019) 573–582. https://doi.org/10.1016/j.jclepro.2019.03.230.
[66] J.W. Brockgreitens, F. Heidari, A. Abbas, Versatile Process for the Preparation of Nanocomposite Sorbents: Phosphorus and Arsenic Removal, Environ. Sci. Technol. 54 (2020) 9034–9043. https://doi.org/10.1021/acs.est.9b07944.
[67] D. Kwak, H. Ra, J. Yang, M. Jeong, A. Lee, W. Lee, J.Y. Hwang, J. Lee, J. Lee, Recovery Mechanism of Degraded Black Phosphorus Field-Effect Transistors by 1,2-Ethanedithiol Chemistry and Extended Device Stability, Small. 14 (2018) 1703194. https://doi.org/10.1002/smll.201703194.
[68] S. Kim, J.-Y. Lee, C.-H. Lee, G.-H. Lee, J. Kim, Recovery of the Pristine Surface of Black Phosphorus by Water Rinsing and Its Device Application, ACS Appl. Mater. Interfaces. 9 (2017) 21382–21389. https://doi.org/10.1021/acsami.7b04728.